Escherichia coli Lipoyl Synthase Binds Two Distinct [4Fe−4S] Clusters per Polypeptide †

ARTICLE *in* BIOCHEMISTRY · OCTOBER 2004

Impact Factor: 3.02 · DOI: 10.1021/bi0488505 · Source: PubMed

Escherichia coli Lipoyl Synthase Binds Two Distinct [4Fe−4S] Clusters per Polypeptide†

Robert M. Cicchillo,‡ Kyung-Hoon Lee,‡ Camelia Baleanu-Gogonea,‡ Natasha M. Nesbitt,‡ Carsten Krebs,*,‡,§ and Squire J. Booker*,‡

Department of Biochemistry and Molecular Biology and Department of Chemistry, The Pennsylvania State University, University Park, Pennsylvania 16802

Received June 3, 2004; Revised Manuscript Received July 14, 2004

ABSTRACT: Lipoyl synthase (LS) is a member of a recently established class of metalloenzymes that use *S*-adenosyl-L-methionine (SAM) as the precursor to a high-energy 5′-deoxyadenosyl 5′-radical (5′-dA•). In the LS reaction, the 5′-dA• is hypothesized to abstract hydrogen atoms from C-6 and C-8 of protein-bound octanoic acid with subsequent sulfur insertion, generating the lipoyl cofactor. Consistent with this premise, 2 equiv of SAM is required to synthesize 1 equiv of the lipoyl cofactor, and deuterium transfer from octanoyl-d_{15} H-protein of the glycine cleavage system—one of the substrates for LS—has been reported [Cicchillo, R. M., Iwig, D. F., Jones, A. D., Nesbitt, N. M., Baleanu-Gogonea, C., Souder, M. G., Tu, L., and Booker, S. J. (2004) *Biochemistry 43*, 6378−6386]. However, the exact identity of the sulfur donor remains unknown. We report herein that LS from *Escherichia coli* can accommodate two [4Fe−4S] clusters per polypeptide and that this form of the enzyme is relevant to turnover. One cluster is ligated by the cysteine amino acids in the C−X_3−C−X_2−C motif that is common to all radical SAM enzymes, while the other is ligated by the cysteine amino acids residing in a C−X_4−C−X_5−C motif, which is conserved only in lipoyl synthases. When expressed in the presence of a plasmid that harbors an *Azotobacter vinelandii isc* operon, which is involved in Fe/S cluster biosynthesis, the as-isolated wild-type enzyme contained 6.9 ± 0.5 irons and 6.4 ± 0.9 sulfides per polypeptide and catalyzed formation of 0.60 equiv of 5′-deoxyadenosine (5′-dA) and 0.27 equiv of lipoylated H-protein per polypeptide. The C68A−C73A−C79A triple variant, expressed and isolated under identical conditions, contained 3.0 ± 0.1 irons and 3.6 ± 0.4 sulfides per polypeptide, while the C94A−C98A−C101A triple variant contained 4.2 ± 0.1 irons and 4.7 ± 0.8 sulfides per polypeptide. Neither of these variant proteins catalyzed formation of 5′-dA or the lipoyl group. Mössbauer spectroscopy of the as-isolated wild-type protein and the two triple variants indicates that greater than 90% of all associated iron is in the configuration $[4Fe-4S]^{2+}$. When wild-type LS was reconstituted with ^{57}Fe and sodium sulfide, it harbored considerably more iron (13.8 ± 0.6) and sulfide (13.1 ± 0.2) per polypeptide and catalyzed formation of 0.96 equiv of 5′-dA and 0.36 equiv of the lipoyl group. Mössbauer spectroscopy of this protein revealed that only ∼67% ± 6% of the iron is in the form of $[4Fe-4S]^{2+}$ clusters, amounting to 9.2 ± 0.4 irons and 8.8 ± 0.1 sulfides or 2 $[4Fe-4S]^{2+}$ clusters per polypeptide, with the remainder of the iron occurring as adventitiously bound species. Although the Mössbauer parameters of the clusters associated with each of the variants are similar, EPR spectra of the reduced forms of the cluster show small differences in spin concentration and *g*-values, consistent with each of these clusters as distinct species residing in each of the two cysteine-containing motifs.

Lipoic acid is best known as a required cofactor in several multienzyme complexes that are involved in the oxidative decarboxylation of α-keto acids and glycine. These include the pyruvate dehydrogenase complex (PDC),[1] the α-ketoglutarate dehydrogenase complex (KDC), the branched-chain oxo-acid dehydrogenase complex (BCDC), and the glycine cleavage system (GCS). In each of these systems, the lipoyl

† This work was supported by a grant from the National Institutes of Health (Grant GM-63847) to S.J.B., by an NIH minority predoctoral fellowship (Grant GM-64033) to N.M.N., and by the "Center for the Study of Biometals in Health and Disease" supported by the Tobacco Settlement Formula (Grant 417−12HY TSF) to C.K.

* To whom correspondence should be addressed. Squire J. Booker, 330 South Frear Laboratory, University Park, PA 16802. Phone: 814-865-8793. Fax: 814-863-7024. E-mail: sjb14@psu.edu. Carsten Krebs, 306 South Frear Laboratory, University Park, PA. 16802. Phone: 814-865-6089. Fax: 814-863-7024. E-mail: ckrebs@psu.edu.

‡ Department of Biochemistry and Molecular Biology.

§ Department of Chemistry.

[1] Abbreviations: 68−73−79, LS C68A−C73A−C79A triple variant; 94−98−101, LS C94A−C98A−C101A triple variant; AI, as-isolated; ARR, *E. coli* anaerobic ribonucleotide reductase; BCDC, branched-chain oxo-acid dehydrogenase complex; BS, biotin synthase; 5′-dA, 5′-deoxyadenosine; 5′-dA•, 5′-deoxyadenosyl 5′-radical; DTB, dethiobiotin; EPR, electron paramagnetic resonance; Fe/S, iron−sulfur; Flv, flavodoxin; Flx, flavodoxin reductase; GCS, glycine cleavage system; HEPES, *N*-(2-hydroxyethyl)piperazine-*N*′-(2-ethanesulfonic acid); KDC, α-ketoglutarate dehydrogenase complex; LS, lipoyl synthase; Ni−NTA, nickel nitrilotriacetic acid; PFL, pyruvate formate-lyase; PCR, polymerase chain reaction; PDC, pyruvate dehydrogenase complex; PLP, pyridoxal 5′-phosphate; RCN, reconstituted; SAM, *S*-adenosyl-L-methionine; WT, wild-type.

10.1021/bi0488505 CCC: $27.50
Published on Web 08/25/2004

Scheme 1: LS-Dependent Conversion of [Octanoyl]H-Protein to [Dihydrolipoyl]H-Protein

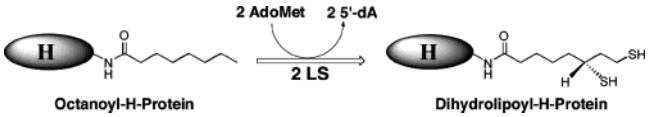

cofactor is bound in an amide linkage to the ϵ-amino group of a conserved lysine residue of the lipoyl-accepting subunit of the respective complex, resulting in a long 14 Å tether, which allows the cofactor to channel intermediates between successive active sites. In each complex, the active form of the cofactor contains a 1,2-dithiolane ring, which undergoes reduction to the dihydrolipoyl form concomitant with turnover. Lipoamide dehydrogenase, one of the components of the complexes, oxidizes the cofactor back to the cyclic disulfide form with concomitant reduction of nicotinamide adenine dinucleotide (NAD^+) (*1*−*7*).

In contrast to the well-known thiamin diphosphate-dependent mechanisms for decarboxylation of α-keto acids by the PDC, KDC, and BCDC (*4*, *6*), the decarboxylation of glycine by the GCS takes place on the P-protein via a pyridoxal 5′-phosphate (PLP)-dependent reaction. After decarboxylation, an aminomethyl group is transferred to the lipoyl cofactor, which resides on a 14 kDa protein called the H-protein. The T-protein catalyzes the cleavage of the amino functionality from the aminomethyl group with concomitant use of the methylene carbon to synthesize N^5,N^{10}-methylenetetrahydrofolate (THF) (*2*, *3*, *8*−*13*).

In *Escherichia coli* and many other organisms, the lipoyl cofactor can be installed by at least two pathways (*14*). Lipoate protein ligase (LplA) catalyzes the activation and transfer of free lipoic acid to the relevant lysine acceptor (*15*, *16*). Alternatively, the lipoyl cofactor can be synthesized endogenously (*14*). The eight-carbon backbone of the cofactor is created via the fatty acid biosynthetic pathway as an appendage to the acyl carrier protein (ACP) (*14*, *17*). LipB, a lipoyl(octanoyl)-acyl carrier protein *N*-lipoyl(octanoyl)transferase (*18*, *19*), catalyzes the transfer of the octanoyl chain from octanoyl-ACP to a target lysine acceptor, affording octanoyl-E2, as in the case of the PDC (*20*)—and, by inference, the KDC and BCDC—and octanoyl H-protein, as in the case of the GCS (*21*). In the second step, lipoyl synthase (LS) mediates insertion of both sulfur atoms into the C-6 and C-8 positions of the appended alkyl chain (Scheme 1) (*20*−*22*).

LS is a member of the radical SAM superfamily of enzymes, which use *S*-adenosyl-L-methionine (SAM) as a precursor to a 5′-deoxyadenosyl 5′-radical (5′-dA•) (*23*−*26*). In each enzyme system, the 5′-dA• initiates catalysis by abstracting a hydrogen atom from a small-molecule substrate or protein. In the former case, this event triggers turnover. In the latter case, the hydrogen is abstracted from the α-carbon of a target glycine residue, creating a glycyl radical cofactor. All characterized members of the radical SAM superfamily have a $C-X_3-C-X_2-C$ motif, in which the designated cysteine amino acids coordinate a [4Fe−4S] cluster that is requisite for turnover. The cluster serves at least two functions: it acts as the immediate donor of one electron, which is required for the reductive cleavage of SAM to generate the 5′-dA• (*27*−*30*), and it acts as a substrate binding determinant, wherein the α-amino and α-carboxylate groups of SAM coordinate in a bidentate fashion to one of the irons (*31*−*37*). The remaining product of SAM cleavage is L-methionine.

In the LS reaction, it is generally believed that the role of the 5′-dA• is to remove hydrogen atoms from the C-6 and C-8 positions of protein-bound derivatives of octanoic acid, allowing for subsequent sulfur insertion (*20*−*22*, *38*, *39*). Consistent with this premise, 2 equiv of SAM is required to synthesize 1 equiv of the lipoyl cofactor, and deuterium transfer from octanoyl-d_{15} H-protein (OHP) to 5′-deoxyadenosine (5′-dA) has been observed (*21*). The nature of the immediate sulfur donor is unknown; however, in vitro studies of the LS reaction are consistent with the premise that the protein itself provides both sulfur atoms: lipoylated proteins can be synthesized in the absence of added compounds that contain sulfur, except for SAM (*21*, *22*), and LS catalyzes less than one turnover in a pseudo-first-order kinetic process, consistent with depletion of the sulfur source (*21*).

There are similarities between LS and biotin synthase (BS), a related radical SAM enzyme that catalyzes the final step in the biotin biosynthetic pathway, the insertion of one sulfur atom between C-6 and C-9 of the substrate, dethiobiotin (DTB) (*40*−*43*). The two proteins from *E. coli* possess 40% sequence similarity and 17% sequence identity, and each contains six conserved cysteine residues (*44*−*46*). In LS, these residues lie in two defined motifs, the $C-X_3-C-X_2-C$ motif that is common to all radical SAM enzymes and a $C-X_4-C-X_5-C$ motif, which is conserved only among lipoyl synthases. In BS, the conserved cysteines that are not part of the radical SAM motif are found scattered throughout the entire polypeptide rather than in a short stretch of amino acids. All six of the conserved cysteines in BS are required for turnover (*47*), and there appears to be universal agreement as to the role of the three residing in the $C-X_3-C-X_2-C$ motif; however, two competing working hypotheses have been advanced regarding the function of the remaining three. On one hand, they are believed to coordinate a [2Fe−2S] cluster that functions in some uncharacterized manner to deliver the sulfur atom in biotin. Consistent with this proposal, a number of laboratories have provided spectroscopic (UV−visible, Mössbauer, EPR, and resonance Raman spectroscopy) and X-ray crystallographic evidence that this cluster form is present in as-isolated (AI) BS, which is inactive, as well as BS that is reconstituted (RCN) to contain a [2Fe−2S] cluster and a [4Fe−4S] cluster, purported to be the active form of the enzyme (*48*−*53*). Moreover, the [2Fe−2S] cluster has been shown to be present in the host bacterium during expression of BS (*54*, *55*), as well as on BS that has been isolated anaerobically (*50*), suggesting that it is not a degradation product of the [4Fe−4S] cluster. On the other hand, another laboratory has reported that BS exhibits cysteine desulfurase activity and that the three remaining cysteines of the protein participate in some uncharacterized manner in liberating sulfur from cysteine and activating it for delivery into dethiobiotin (*56*). Consistent with this proposal, a requirement for PLP and the presence of a cysteine persulfide on BS has been demonstrated (*56*).

In this work, we show that LS can accommodate two [4Fe−4S] clusters. One is coordinated by the $C-X_3-C-X_2-C$ motif that is common among radical SAM enzymes and is proposed to function in generating the 5′-dA•. The second cluster is housed in the $C-X_4-C-X_5-C$ motif,

Table 1: Sequence of Primers Used in Cloning and Mutagenesis

primer	sequence[a]	use
AS005	5′-AAA CGT TGC GGT ACC GTG GTT GAA **CGC** TTC CGC-3′	reverse PCR primer for C79A mutation
AS006	5′-AAA CGT TGC GGT ACC GTG GTT GAA GCA TTC CGC CAG GTT AGG **CGC** GGA GGC-3′	reverse PCR primer for C73A mutation
AS007	5′-AAA CGT TGC GGT ACC GTG GTT GAA GCA TTC CGC CAG GTT AGG GCA GGA GGC TTC CTC **CGC** GAC AGA-3′	reverse PCR primer for C68A mutation
CG002	5′-GTG GGC GAC GTC ACA GAA CGG ACA ACG GCG GGT **AGC** AAT AGC-3′	reverse PCR primer for C94A mutation
JE002	5′-GAG GAT CAT AAA CGT TGC *GGT ACC* GTG GTT GAA GCA TTC CGC-3′	reverse PCR primer for *Kpn*I silent mutation
JE001	5′-GCG GAA TGC TTC AAC CAC *GGT ACC* GCA ACG TTT ATG ATC CTC-3′	forward PCR primer for *Kpn*I silent mutation
AatIIfor	5′-CCG TTC TGT *GAC GTC* GCC CAC GGT CGG CCG-3′	forward PCR primer for *Aat*II silent mutation
AatIIrev	5′-CGG CCG ACC GTG GGC *GAC GTC* ACA GAA CGG-3′	reverse PCR primer for *Aat*II silent mutation
KHL001	5′-CGC CGT **GCT** CCG TTC **GCT** GAC GTC GCC CAC GGT CGG-3′	forward primer for C94A−C98A−C101A triple variant[b]
KHL002	5′-CCG ACC GTG GGC GAC GTC **AGC** GAA CGG **AGC** ACG GCG-3′	reverse primer for C94A−C98A−C101A triple variant[b]
SB004	5′-GCG GCG TC*C ATA TG*A GTA AAC CCA TTG TGA TGG AAC GC-3′	forward PCR primer for cloning lipoyl synthase
SB002	5′-GCC G*GA ATT C*TT ACT TAA CTT CCA TCC CTT TCG C-3′	reverse PCR primer for cloning lipoyl synthase

[a] Italic-type bases designate engineered restriction sites, while bold-type bases designate altered codons. [b] Mutagenesis carried out using QuikChange kit from Stratagene in combination with the C94A template.

which is unique to lipoyl synthases. We speculate that this cluster somehow functions to deliver the sulfur that is incorporated into the product. We show that both clusters are required for turnover, and, importantly, that formation of product, lipoyl H-protein (LHP), does not require reconstitution of LS.

MATERIALS AND METHODS

Materials. All DNA modifying enzymes and reagents were purchased from New England Biolabs (Beverly, MA), as was Vent polymerase and its associated 10× reaction buffer. Oligonucleotide primers for cloning and mutagenesis were obtained from Integrated DNA Technologies (Coralville, IA) or Invitrogen Life Technologies (Carlsbad, CA). Both the Bradford reagent for protein concentration determination and the bovine serum albumin (BSA) standard (2 mg mL^{-1}) were obtained from Pierce (Rockford, IL). *E. coli* genomic DNA (strain W3110) was obtained from Sigma Corp (St. Louis, MO). All other buffers and common chemicals were reagent grade or better.

^{57}Fe (97−98%) metal was purchased from Pennwood Chemicals (Great Neck, NY). It was washed with $CHCl_3$ and dissolved with heating in an anaerobic solution of 2 N H_2SO_4 (1.5 mol of H_2SO_4 per mole of ^{57}Fe). It was used as is for bacterial growths. For reconstitution experiments, it was first titrated to pH 6.5 with an anaerobic solution of saturated sodium bicarbonate. Routine iron and sulfide analysis was conducted as described previously (*57*−*59*).

Spectroscopic Methods. UV−visible spectra were recorded using Cary 50 or Cary 300 spectrometers (Varian; Walnut Creek, CA) in combination with the associated WinUV software package. Low-temperature X-band EPR spectroscopy was carried out in perpendicular mode on a Bruker (Billerica, MA) ESP 300 spectrometer equipped with an ER 041 MR microwave bridge and an ST4102 X-band resonator (Bruker). Sample temperature was maintained with an ITC503S temperature controller and an ESR900 liquid helium cryostat (Oxford Instruments; Concord, MA). Spin concentration was determined by double integration of the sample spectrum and comparing the resulting intensity to that of a 1 mM $CuSO_4$/10 mM EDTA standard run under identical conditions. General spectral manipulations were carried out using the program IGOR Pro (Wavemetrics, Lake Oswego, OR) on a desktop computer.

Mössbauer spectra were recorded on spectrometers from WEB research (Edina, MN) operating in the constant acceleration mode in a transmission geometry. Spectra were recorded with the temperature of the sample maintained at 4.2 K. For low-field spectra, the sample was kept inside an SVT-400 dewar from Janis (Wilmington, MA), and a magnetic field of 40 mT was applied parallel to the γ-beam. For high-field spectra, the sample was kept inside a 12SVT dewar (Janis), which houses a superconducting magnet that allows for application of variable magnetic fields between 0 and 8 T parallel to the γ-beam. The quoted isomer shifts are relative to the centroid of the spectrum of a metallic foil of α-Fe at room temperature. Data analysis was performed using the program WMOSS from WEB research.

Recombinant DNA Procedures. The polymerase chain reaction was performed with a Robocycler (Stratagene) temperature cycler. Each amplification reaction contained the following in a volume of 100 μL: 50 pmol of each primer, 20 nmol of each deoxynucleoside triphosphate, 1 μg of *E. coli* genomic DNA, 1 U of Vent polymerase, and 10 μL of 10× Vent polymerase buffer. After a 5 min denaturation step at 95 °C, 35 cycles of the following program were initiated: 1 min at 95 °C, 1 min at 45 °C, and 3 min at 72 °C. All other procedures were carried out by standard methods (*60*). DNA sequencing was carried out at the Pennsylvania State University Nucleic Acid Facility.

Construction of the C68A−C73A−C79A Triple Variant. The cloning of wild-type LS into expression vector pET-28a has already been described (*21*). Single, double, and triple variants of cysteines 68, 73, and 79 were constructed by PCR using the primers listed in Table 1. Initially, a silent *Kpn*I restriction site was engineered into the gene sequence for LS at positions 247−252 by changing a cytosine at position 249 to a thymine, and an adenine at position 252 to a cytosine. These alterations converted the naturally encoded GGC ACA to GGT ACC, with no change in the encoded

glycine and threonine amino acids. The *lipA* gene was amplified in two halves with primer JE001 in combination with primer SB002 and primer JE002 in combination with primer SB004. After purification of the resulting fragments and digestion with *Nde*I and *Kpn*I (for the fragment amplified with primers SB004 and JE002) or *Eco*RI and *Kpn*I (for the fragment amplified with primers SB002 and JE001), the two fragments were simultaneously ligated into a pET-28a expression vector that had been digested with *Nde*I and *Eco*RI. The resulting construct was used as the template for construction of the C68A−C73A−C79A triple variant by PCR using primers AS007, AS006, and AS005—all of which spanned the engineered *Kpn*I restriction site—in combination with primer SB004. Construction of the C68A single variant generated the template for construction of the C68A−C73A double variant; the double variant was then used as the template for construction of the C68A−C73A−C79A triple variant. After amplification by PCR, the resulting fragments were digested with *Nde*I and *Kpn*I, and simultaneously ligated into pET-28a along with the fragment that was amplified with primers SB002 and JE001.

Construction of the C94A−C98A−C101A Triple Variant. Single, double, and triple variants of cysteines 94, 98, and 101 were constructed by PCR using primers listed in Table 1. A silent *Aat*II restriction site was engineered into the *lipA* gene at positions 304−309 by converting a thymine at position 309 to a cytosine. This alteration converted the naturally encoded GAC GTT to GAC GTC with no change in the encoded valine amino acid. The *lipA* gene was amplified in two halves with primer AatIIfor in combination with SB002 and primer AatIIrev in combination with SB004. After purification of the resulting fragments and digestion with *Nde*I and *Kpn*I (for the fragment amplified with primers SB004 and AatIIrev) or *Eco*RI and *Eco*RI (for the fragment amplified with primers SB002 and AatIIfor), the two fragments were simultaneously ligated into pET-28a that had been digested with *Nde*I and *Kpn*I. The resulting construct was then used as the template for the construction of the C94A single variant using primer CG002, which spanned the engineered *Aat*II restriction site, in combination with primer SB004. For uncharacterized reasons, construction of the double and triple variants was resistant to this strategy. The triple variant was therefore synthesized using the QuikChange site-directed mutagenesis kit from Stratagene in combination with primers KHL001 and KHL002, and the C94A single variant as template. The procedure was carried out according to the protocol established by the manufacturer but amended as described by Ramamurthy et al. (*61*). The expression of both triple variants was carried out in minimal media and in the presence of plasmid pDB1282 as previously described (*21*), except that ^{57}Fe was added to the growth media instead of natural abundance iron. The purification and reconstitution of wild-type and variant proteins was carried out as previously described (*21*), except that ^{57}Fe was used for the reconstitution instead of natural abundance iron.

Extinction Coefficient Determination and Bradford Protein Assay Standardization for LS. Protein concentrations of LS samples were analyzed in triplicate by the Bradford dye-staining procedure (Pierce) with BSA as the standard. Parallel samples were also subjected to quantitative amino acid analysis at the University of Iowa's Molecular Analysis Facility. The average protein concentration obtained from the samples subjected to amino acid analysis was then used to determine a correction factor for the Bradford assay.

Preparation of Mössbauer and EPR Samples. Samples to be analyzed by Mössbauer and EPR spectroscopies were prepared inside of the anaerobic chamber and contained 200−1300 μM LS. Samples (300 μL final volume) to be analyzed by Mössbauer spectroscopy were frozen with liquid nitrogen inside of small plastic cups. For characterization by EPR, the samples (250 μL final volume) were first treated with 2 mM sodium dithionite at ambient temperature for ~2 min, placed in EPR tubes (2 mm i.d.), and frozen in liquid nitrogen. All steps associated with preparing the samples were conducted inside of a Coy Laboratory Products (Grass Lake, MI) anaerobic chamber.

RESULTS

Expression and Purification of Wild-Type and Variant E. coli LS Proteins. All wild-type and variant LS proteins in this study were coexpressed with plasmid pDB1282 in ^{57}Fe-containing M9 minimal media as described previously (*21*). Plasmid pDB1282 carries an *A. vinelandii* operon that is believed to be important in the biosynthesis of Fe/S clusters. This operon contains the genes *iscS*, *iscU*, *iscA*, *hscA*, *hscB*, and *fdx* (*62*−*64*) cloned behind an arabinose-inducible promoter in a plasmid that confers ampicillin resistance, while the pET-28a plasmid into which the WT and variant *lipA* genes were cloned confers resistance to kanamycin. The proteins were isolated by immobilized metal affinity chromatography (IMAC) as previously described (*21*), exploiting the hexahistidine tag that is appended to the N-terminus of each.

Quantitative amino acid analysis was employed to establish an extinction coefficient for as-isolated LS and to standardize the Bradford protein assay. Because the protein has a propensity to precipitate in the presence of oxygen, which could compromise the accuracy of the result, care was taken to ensure that the solution was indeed homogeneous while transferring it to hydrolysis tubes. In seven analyses, performed on two separate occasions (triplicate and quadruplicate), concentrations of various amino acids were used in conjunction with the published amino acid sequence to quantify the LS concentration after hydrolysis of the protein. Using a commercially available BSA standard, the concentration of which was verified by UV−visible spectroscopy ($\epsilon^{1\%} = 6.67$), we determined that the Bradford protein assay overestimates the concentration of LS by a factor of 1.47 ± 0.27. Determination of the molar absorptivity at 400 nm of the various Fe/S cluster species associated with LS cannot be accomplished from UV−visible data alone but also requires analytical information and analysis by Mössbauer and EPR spectroscopies, which can be used to observe and quantify all of the relevant iron-containing species.

Analytical and Spectroscopic Characterization of AI WT LS. The UV−visible spectrum of AI LS coexpressed in ^{57}Fe-containing minimal media in the presence of plasmid pDB1282 and purified under anaerobic conditions as described previously (*21*) is displayed in Figure 1A (solid line). In addition to the peak at 280 nm, the spectral envelope contains a small shoulder at 330 nm and a broad peak at 400 nm, which tails out beyond 700 nm. These features, as well as the dark brown color of the protein, are consistent

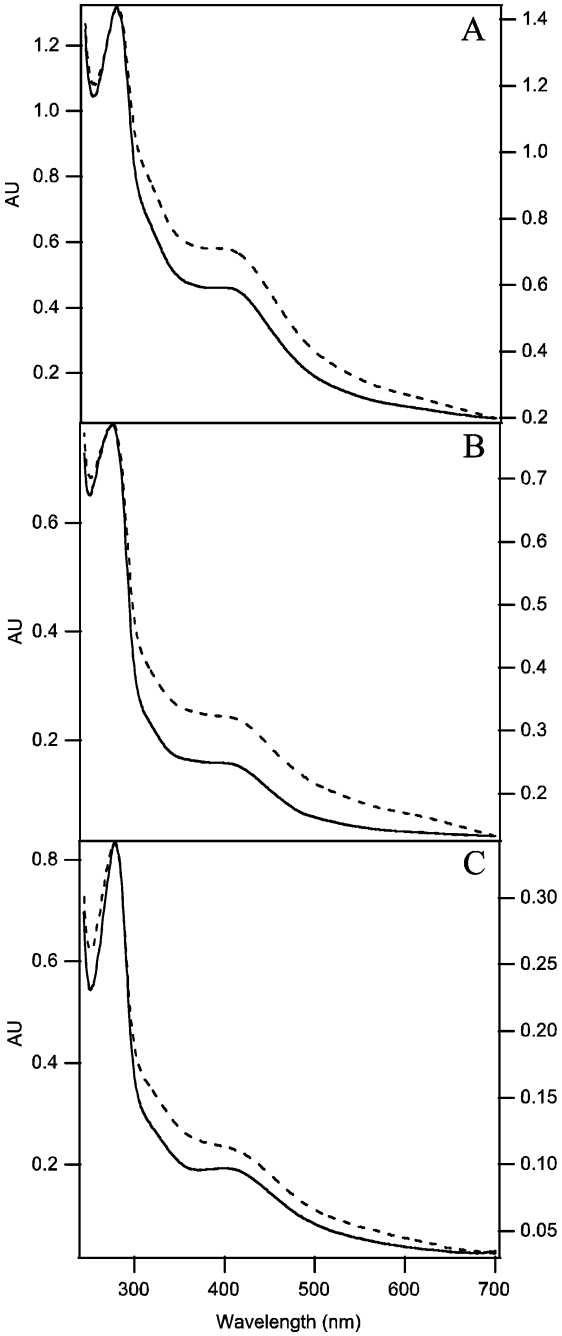

FIGURE 1: UV-visible spectra of (A) WT LS, (B) 94−98−101, and (C) 68−73−79. In each case, the solid line represents the as-isolated sample, while the dashed line represents the reconstituted sample. Sample concentrations were 21.2 μM for AI WT LS, 17.2 μM for RCN WT LS, 13.0 μM for AI 94−98−101, 9.08 μM for RCN 94−98−101, 19.8 μM for AI 68−73−79, and 6.25 μM for RCN 68−73−79. For each spectrum, the secondary *Y*-axis corresponds to the absorbance for the reconstituted proteins.

with the presence of Fe/S clusters. Although it is difficult to predict accurately the type of clusters associated with the protein solely from UV−visible spectroscopy, the spectrum is distinct from that of AI BS, as well as the reconstituted form of the protein that gives rise to turnover (*48*−*52*, *65*). In particular, the UV−visible spectrum of LS lacks the telltale features of $[2Fe-2S]^{2+}$ clusters, a broad peak at ∼460 nm, as well as a shoulder at ∼550 nm that is sometimes observed (*50*, *65*−*68*). The protein shown in Figure 1A (solid line) contained 6.9 ± 0.5 equiv of Fe and 6.4 ± 0.9 equiv

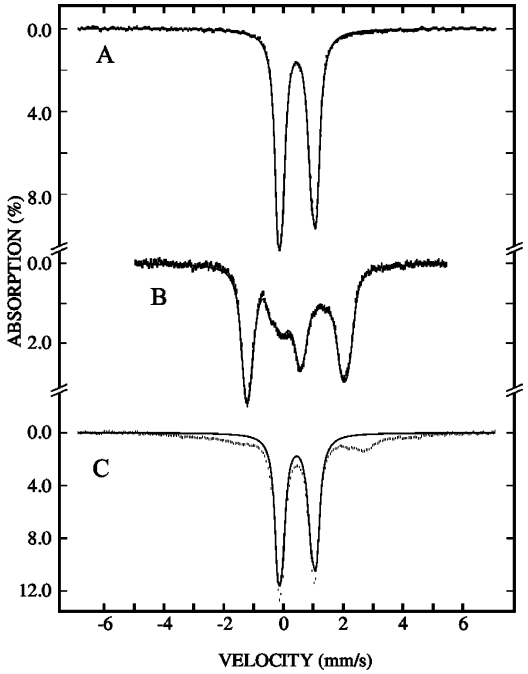

FIGURE 2: Mössbauer spectra of WT AI LS recorded at 4.2 K in an externally applied field (oriented parallel to the γ-beam) of (A) 40 mT and (B) 8 T. The solid line overlaid with the experimental data (hash marks) are simulations representing the contribution from the $[4Fe-4S]^{2+}$ clusters using the parameters given in the text. The Mössbauer spectrum of WT RCN LS recorded at 4.2 K in an externally applied field (oriented parallel to the γ-beam) of 40 mT is shown in panel C. The simulation of the $[4Fe-4S]^{2+}$ clusters, scaled to 70% of the total intensity of spectrum C is shown as a solid line.

of S^{2-} per polypeptide. This stoichiometry is a little less than 2-fold greater than that previously reported for WT LS (*22*, *39*, *64*), as well as that which we observe when the protein is isolated from an expression host that does not contain the accessory plasmid (data not shown). Consistent with the greater stoichiometry of Fe and S^{2-} associated with LS, the A_{280}/A_{400} ratio in this preparation is 2.88. The A_{280}/A_{400} ratio of AI LS purified in the absence of plasmid pDB1282 is typically ∼4.

The Mössbauer spectrum of a sample of AI WT LS recorded at 4.2 K in an externally applied magnetic field (40 mT) oriented parallel to the γ-beam is shown in Figure 2A. It shows two broad lines at −0.12 mm/s and +1.04 mm/s, which belong to a quadrupole doublet having parameters (isomer shift δ = 0.46 mm/s and quadrupole splitting parameter ΔE_Q = 1.16 mm/s) that are typical of $[4Fe-4S]^{2+}$ clusters. Because the width of the lines is rather large, the spectrum was analyzed assuming two quadrupole doublets of equal intensity, yielding the following parameters: isomer shifts $\delta(1)$ = 0.45 and $\delta(2)$ = 0.46 mm/s and quadrupole splitting parameters $\Delta E_Q(1)$ = 0.98 and $\Delta E_Q(2)$ = 1.30 mm/s. These two quadrupole doublets account for 97% ± 3% of the total intensity of the spectrum, and the associated parameters are typical of $[4Fe-4S]^{2+}$-containing proteins. To corroborate this assignment, a spectrum of this sample was recorded at 4.2 K in an 8 T magnetic field (Figure 2B). $[4Fe-4S]^{2+}$ clusters have diamagnetic ground states, and therefore, it is expected that the magnetic field experienced by the ^{57}Fe nuclei would equal the externally applied field (8 T). The solid line overlaid with the experimental data in

Figure 2B is a theoretical spectrum using the parameters obtained from the 40 mT spectrum (asymmetry parameters $\eta(1) = 0.5$ and $\eta(2) = 0.6$) and assuming a diamagnetic ($S = 0$) ground state. We note that detection of small amounts of $[2Fe-2S]^{2+}$ clusters, which typically exhibit a quadrupole doublet with $\delta \approx 0.28$ mm/s and $\Delta E_Q \approx 0.6$ mm/s, is difficult. Including a third quadrupole doublet with parameters typical of $[2Fe-2S]^{2+}$ clusters does not improve the quality of the fit significantly. Furthermore, the parameters of the $[4Fe-4S]^{2+}$ component are essentially the same, and no more than 5% of the total intensity is in the form of $[2Fe-2S]^{2+}$ clusters. We therefore conclude that this sample contains at most 5% of the iron in the form of $[2Fe-2S]^{2+}$ clusters. A previous Mössbauer study of LS revealed the presence of $[4Fe-4S]^{2+}$ and $[2Fe-2S]^{2+}$ clusters in RCN WT LS (*69*). The reported spectrum has a discernible shoulder at ca. 0.6 mm/s, indicative of the high-energy line of the spectrum of $[2Fe-2S]^{2+}$ clusters. We do not see this feature in our spectrum of AI WT LS, which indicates that the percentage of $[2Fe-2S]^{2+}$ clusters in our preparation of LS is smaller.

The EPR spectrum of an identical sample of AI, ^{57}Fe-grown LS reveals the presence of a small amount (14 μM, 0.03 equiv or 1.5% of the total Fe) of a $[3Fe-4S]^{+}$ cluster. This type of cluster gives rise to fairly broad and magnetically split Mössbauer spectra when recorded at 4.2 K in a 40 mT external magnetic field, and therefore, this small amount is not detectable in the spectrum in Figure 2A (*70*). By combining Mössbauer and EPR spectroscopic results with iron and sulfide quantification on the exact same proteins, it can be concluded that AI WT LS contains 1.7 ± 0.2 $[4Fe-4S]^{2+}$ and 0.03 $[3Fe-4S]^{+}$ clusters, consistent with the presence of two distinct [4Fe−4S] cluster binding sites in each polypeptide.

Analytical and Spectroscopic Characterization of RCN WT LS. Upon reconstitution of AI WT LS with ^{57}Fe, the concentrations of iron and sulfide that elute with the desalted protein increase enormously to 13.8 ± 0.6 Fe and 13.1 ± 0.2 S^{2-} per polypeptide. Concomitant with the increase in iron and sulfide content is a change in the UV−visible spectrum of the protein (Figure 1A, dashed line); the region of the spectrum that is characteristic of the Fe/S cluster has increased in amplitude, although no distinct features that would suggest the presence of other cluster forms are observed. In addition, the A_{280}/A_{400} ratio has decreased to 2.04, suggestive of incorporation of additional Fe/S-containing species. As detailed below, we employed Mössbauer spectroscopy to determine the configuration and stoichiometry of these additional Fe/S-containing species.

The Mössbauer spectrum of this sample, recorded at 4.2 K and 40 mT, is shown in Figure 2C. In addition to the two peaks associated with the broad quadrupole doublet emanating from the $[4Fe-4S]^{2+}$ clusters, there is a broad component extending from −5 to +5 mm/s with a pronounced broad absorption at ∼2.8 mm/s. The broad features may originate from paramagnetic Fe/S cluster species, from adventitiously bound ^{57}Fe, or from both. The EPR spectrum of this sample (data not shown) reveals that it contains an insignificantly small amount of $[3Fe-4S]^{+}$ clusters; $[2Fe-2S]^{+}$ and $[4Fe-4S]^{+}$ species are not observed. $[3Fe-4S]^{0}$ clusters could potentially also give rise, at least in part, to the broad features. They have an $S = 2$ ground state and exhibit a significant spin expectation value, even in small externally applied magnetic fields, giving rise to magnetically split Mössbauer spectra (*71*). In the absence of an external magnetic field, however, the spectrum associated with $[3Fe-4S]^{0}$ clusters collapses into quadrupole doublets. We recorded the 4.2 K zero-field spectrum of RCN WT LS (data not shown), and it is identical to that of the spectrum obtained at 4.2 K and 40 mT. Therefore, the broad feature is attributed to adventitiously bound iron. Deconvolution of the Mössbauer spectrum reveals that 67% ± 6% of the total Fe is in the form of $[4Fe-4S]^{2+}$ clusters. The relative amount of this component has a larger uncertainty because the exact shape of the spectral contribution from adventitiously bound iron is not known. These results, when combined with iron and sulfide analysis, suggest that reconstituted LS contains 2.3 ± 0.3 $[4Fe-4S]^{2+}$ clusters per polypeptide, again consistent with the presence of two distinct Fe/S cluster binding sites per polypeptide.

Analytical and Spectroscopic Characterization of the C94A−C98A−C101A Triple Variant. The UV−visible spectrum of the AI C94A−C98A−C101A triple variant (94−98−101), expressed and purified similarly to the WT protein, is displayed in Figure 1B (solid line). The overall spectral envelope is quite similar to that of WT LS, displaying the same distinctive features at 330 and 400 nm but not displaying features that are indicative of $[2Fe-2S]^{2+}$ clusters. Analysis for iron and sulfide yielded 4.2 ± 0.1 equiv of Fe and 4.7 ± 0.8 equiv of S^{2-} per polypeptide, consistent with the premise that one of the [4Fe−4S] cluster binding sites has been removed. However, upon reconstitution with iron and sulfide, the UV−visible spectrum of the triple variant changes significantly (Figure 1B, dashed line), shifting from an A_{280}/A_{400} ratio of 5 in the as-isolated sample to 2.5 in the reconstituted sample, suggesting that additional Fe/S-containing species are incorporated despite deletion of one of the presumed cluster binding motifs.

The Mössbauer spectrum of AI 94−98−101, recorded at 4.2 K and 40 mT, is shown in Figure 3A. It is nearly identical to the spectrum of WT LS, and a fit of the experimental spectrum to two quadrupole doublets yields the following parameters: $\delta(1) = 0.44$, $\delta(2) = 0.46$, $\Delta E_Q(1) = 1.00$, and $\Delta E_Q(2) = 1.33$ mm/s. This component accounts for 97% ± 3% of the total ^{57}Fe in this sample, indicating that nearly all of the iron in the sample is in the configuration $[4Fe-4S]^{2+}$. Additionally, AI 94−98−101 is EPR silent, indicating that the paramagnetic cluster types, $[2Fe-2S]^{+}$, $[4Fe-4S]^{+}$, and $[3Fe-4S]^{+}$, are not present. Spectral analysis in combination with iron and sulfide quantification therefore indicates that AI 94−98−101 contains 1.0 ± 0.1 $[4Fe-4S]^{2+}$ cluster per polypeptide.

The Mössbauer spectrum of RCN 94−98−101 is displayed in Figure 3B. The spectrum shows, in addition to the two lines at −0.12 and +1.04 mm/s of the $[4Fe-4S]^{2+}$ cluster, a broad absorption extending from −5 to +5 mm/s. The shape of this component is similar to that observed in the spectrum of reconstituted WT LS. Again, the reconstituted triple variant is EPR silent at 13 K, demonstrating the absence of paramagnetic Fe/S cluster types. Therefore, the broad absorption is attributed to adventitiously bound Fe. Deconvolution of the spectrum reveals that 38% ± 6% of the total absorption is contributed by the subspectrum of the $[4Fe-4S]^{2+}$ cluster. This percentage in combination with iron

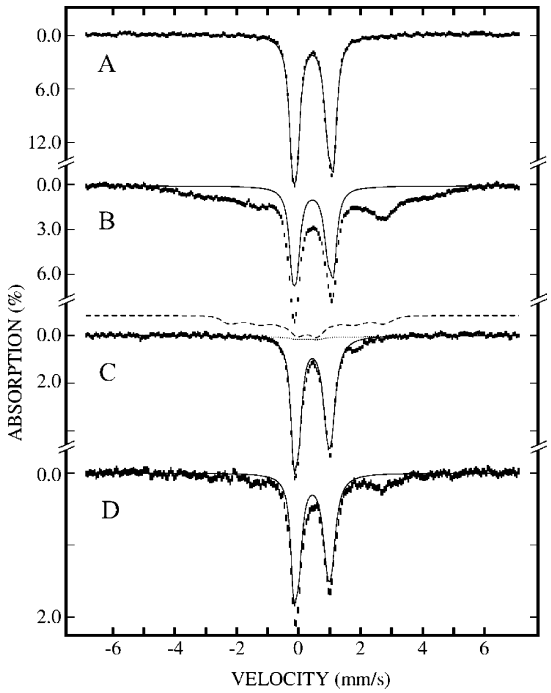

FIGURE 3: Mössbauer spectra recorded at 4.2 K in an externally applied 40 mT magnetic field of (A) AI 94−98−101, (B) RCN 94−98−101, (C) AI 68−73−79, and (D) RCN 68−73−79. The solid lines are simulations of the $[4Fe-4S]^{2+}$ cluster component, using the parameters in the text. The dotted line in panel C is a theoretical simulation of the $[3Fe-4S]^{+}$ cluster scaled to 8% of the total intensity of the experimental spectrum. The dashed line in panel C is the same simulation of the $[3Fe-4S]^{+}$ cluster component, magnified 5-fold for clarity.

and sulfide analysis indicates an overall stoichiometry of 1.0 ± 0.2 $[4Fe-4S]^{2+}$ clusters per 94−98−101 polypeptide. Importantly, reconstitution of the triple variant does not increase the content of $[4Fe-4S]^{2+}$ clusters per polypeptide, strongly corroborating the hypothesis that cysteines 94, 98, and 101 of WT LS coordinate a [4Fe−4S] cluster.

Analytical and Spectroscopic Characterization of the C68A−C73A−C79A Triple Variant. The UV−visible spectrum of the AI C68A−C73A−C79A triple variant (68−73−79), expressed and purified similarly to the WT protein, is displayed in Figure 1C (solid line). Again, the overall spectral envelope is similar to that of WT LS, possessing the same distinctive features at 330 and 400 nm but not displaying features that are indicative of [2Fe−2S] clusters. Analysis for iron and sulfide yielded 3.0 ± 0.2 equiv of Fe and 3.6 ± 0.4 equiv of S^{2-} per polypeptide, enough only to support formation of one $[4Fe-4S]^{2+}$ cluster per polypeptide. The UV−visible spectrum of the AI triple variant when compared to that of the AI WT protein is consistent with this premise. The A_{280}/A_{400} ratio is 4.4, which is similar to that for 94−98−101. Upon reconstitution of AI 68−73−79, the associated UV−visible spectrum changes only mildly, displaying an A_{280}/A_{400} ratio of 3, which is consistent with the changes in iron and sulfide content (4.8 ± 0.1 equiv of Fe and 3.6 ± 0.2 equiv of S^{2-}).

The Mössbauer spectrum of the AI 68−73−79, recorded at 4.2 K and 40 mT, is shown in Figure 3C. It shows three features: two prominent peaks at −0.1 and +1.0 mm/s, indicating the presence of $[4Fe-4S]^{2+}$ clusters, and a broad peak at +1.8 mm/s, which tails out to ∼3 mm/s. We speculate that this peak originates from adventitiously bound iron or from $[3Fe-4S]^{0}$ clusters. As discussed previously, the spectral features of $[3Fe-4S]^{0}$ clusters collapse in zero-field to quadrupole doublets, allowing them to be identified in such a manner. The zero-field spectrum of AI 68−73−79 is identical to the 40 mT spectrum, indicating that the sample does not contain $[3Fe-4S]^{0}$ clusters. We therefore assign the broad feature to adventitiously bound iron.

The EPR spectrum of AI 68−73−79 (data not shown) reveals the presence of a small amount (10 μM or 0.08 equiv, which corresponds to 8% of the total Fe in the sample) of $[3Fe-4S]^{+}$ clusters. For the deconvolution of the Mössbauer spectrum we approximate the contribution of the $[3Fe-4S]^{+}$ clusters by using the simulation of the $[3Fe-4S]^{+}$ clusters observed in pyruvate formate-lyase activating enzyme (PFL-AE), which is another member of the radical SAM superfamily (*72*). The simulation of the $[3Fe-4S]^{+}$ clusters, scaled to 8% of the total intensity, is shown as a dotted line overlaid with the experimental data in Figure 3C. For clarity, we also show the spectrum of this component magnified 5-fold as a dashed line above the spectrum in Figure 3C. For the analysis of the Mössbauer spectrum of AI 68−73−79, we removed the contribution of the $[3Fe-4S]^{+}$ cluster from the raw data, and fitted the resulting spectrum to two quadrupole doublets, representing the $[4Fe-4S]^{2+}$ clusters. This analysis yields the following parameters: $\delta(1) = 0.46$, $\delta(2) = 0.45$, $\Delta E_Q(1) = 0.92$, and $\Delta E_Q(2) = 1.22$ mm/s, accounting for 93% ± 6% of the total iron in this sample. This percentage in combination with results from iron and sulfide analysis indicates that there are 0.7 ± 0.1 $[4Fe-4S]^{2+}$ clusters per polypeptide associated with AI 68−73−79.

The spectrum of RCN 68−73−79 is shown in Figure 3D. In addition to the two prominent lines that are contributed by the $[4Fe-4S]^{2+}$ cluster, there is a broad absorption extending from ca. −3 to +3 mm/s. Again, we attribute this absorption to adventitiously bound iron, since the sample is EPR-silent. The $[4Fe-4S]^{2+}$ cluster component can be simulated using the same parameters that were used to simulate that of AI 68−73−79 and were found to correspond to 70% of the total intensity. This percentage in combination with iron and sulfide analysis results in a stoichiometry of 0.8 ± 0.2 $[4Fe-4S]^{2+}$ clusters per polypeptide. These results are in full agreement with our hypothesis that cysteines 94, 98, and 101 ligate one [4Fe−4S] cluster while cysteines 68, 73, and 79 ligate another. We point out that the addition of the Mössbauer spectra of AI 68−73−79 LS (Figure 3C) and AI 94−98−101 LS (Figure 3A) in a 1:1 ratio closely resembles that of AI WT LS (Figure 2A).

Determination of Extinction Coefficients at 400 nm of WT and Variant Lipoyl Synthases. We have used a combination of analytical methods and Mössbauer spectroscopy to determine the stoichiometry of the various Fe/S-containing species present in the samples of AI and RCN WT and variant LSs. Our finding that the iron in all three AI samples is almost exclusively (>93%) in the form of $[4Fe-4S]^{2+}$ clusters allows a fairly accurate determination of their extinction coefficients at 400 nm. From the protein concentration of AI WT LS ($(2.1 \pm 0.4) \times 10^{-5}$ M) determined from the corrected Bradford protein assay, the absorbance at 400 nm (0.461), and the stoichiometry of $[4Fe-4S]^{2+}$ clusters per polypeptide (1.7 ± 0.2) as determined from analytical methods and Mössbauer analysis, we calculate an

average ϵ_{400} of 12 800 ± 2816 M^{-1} cm^{-1} for each of the $[4Fe-4S]^{2+}$ clusters. The same analysis yields ϵ_{400} = 13 900 ± 3058 M^{-1} cm^{-1} for AI 68−73−79 LS and ϵ_{400} = 12 200 ± 2684 M^{-1} cm^{-1} for AI 94−98−101 LS. These values fall into the range of molar absorptivities that have been observed for peptide-ligated $[4Fe-4S]^{2+}$ model complexes in organic solvents, for which ϵ_{400} values of 12 100−17 500 M^{-1} cm^{-1} have been reported (*66*, *67*).

EPR Spectroscopy of WT, 68−73−79, and 94−98−101 LS. The EPR spectrum of AI WT LS, reduced in the presence of 2 mM sodium dithionite, is shown in Figure 4A (solid line). The spectrum, which was obtained at 13 K and 5 mW power, exhibits a pseudoaxial signal that is broad and distorted with a **g**-tensor that is approximated by the principal values $g_{\|}$ = 2.03 and $g_{\perp}$ = 1.93. Additionally, there is a shoulder at g = 1.99 (arrow). The EPR spectrum of the dithionite-reduced RCN WT LS is also shown in Figure 4A (dotted line) and exhibits features that are quite similar to that of the AI protein, if not identical. Spin quantification using a Cu-EDTA standard indicated that both signals accounted for 0.08−0.09 equiv of spin per equivalent of polypeptide. In addition, both signals were of maximum intensity at 13 K and diminished greatly in intensity at temperatures above 40 K at 5 mW power (data not shown), consistent with the presence of $[4Fe-4S]^{+}$ clusters.

The EPR spectrum of dithionite-reduced AI 94−98−101 is shown in Figure 4B (solid line); the spectrum of dithionite-reduced WT LS is also displayed (dotted line) for comparison. The spectrum, which was recorded on a 1.3 mM sample of the triple variant, is visibly weak in intensity and accounts for less than 0.001 equiv of spin per polypeptide, indicating that the $C-X_4-C-X_5-C$ cluster is not readily reduced in the presence of 2 mM dithionite. The shape of the spectrum is different from that of the WT protein, exhibiting more axial character with **g**-tensor principal values that are approximated by $g_{\|}$ = 2.05 and $g_{\perp}$ = 1.91.

The EPR spectrum of dithionite-reduced AI 68−73−79 is shown in Figure 4C (solid line); the spectrum of dithionite-reduced WT LS is also displayed (dotted line). This spectrum better approximates that of WT LS than that of 94−98−101, displaying a **g**-tensor with principal values that are approximated by $g_{\|}$ = 2.03 and $g_{\perp}$ = 1.93. Interestingly, the shoulder at g = 1.99 is absent, which may reflect small conformational differences of the radical SAM [4Fe−4S] cluster in WT LS and 68−73−79. We also note that the EPR spectrum of WT LS may also be perturbed as a consequence of dipolar coupling between the two $[4Fe-4S]^{+}$ clusters. The overall low yield of reduction, however, would result in only a small fraction of WT LS that would have both [4Fe−4S] clusters reduced, suggesting that the feature at g = 1.99 is not attributable to dipolar coupling. The spectrum of AI 68−73−79 also resembles that of the reduced activating proteins of *E. coli* anaerobic ribonucleotide reductase (ARR) and PFL (*30*, *73*), as well as reduced BS (*69*). This is consistent with the premise that cysteines 94, 98, and 101 coordinate the Fe/S cluster that resides in the radical SAM motif.

Turnover of WT and Variant Lipoyl Synthases. Wild-type LS and the two triple variants were assayed for their ability to cleave SAM and synthesize LHP from the OHP substrate as described in a previous publication (*21*). As shown in Table 2, neither of the triple variants was capable of

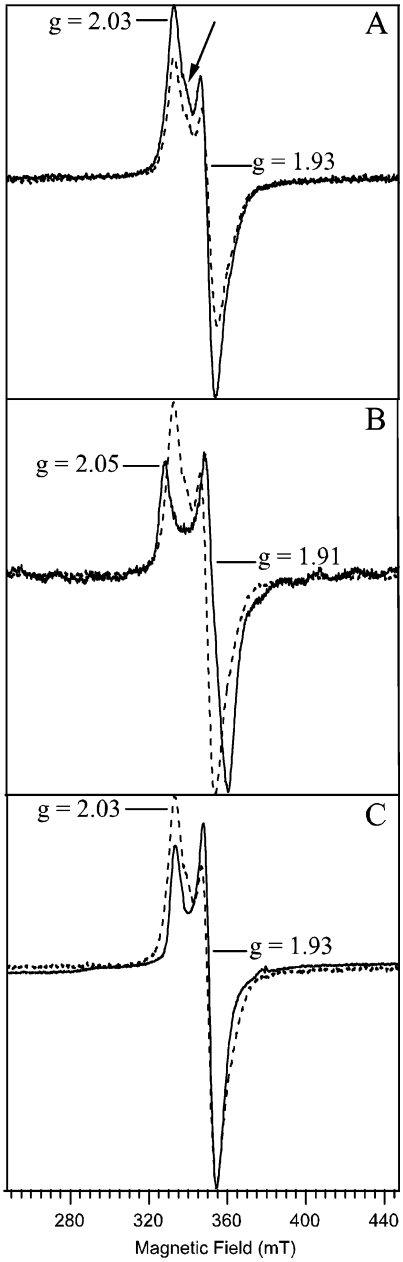

FIGURE 4: EPR spectra of (A) WT LS, (B) 94−98−101, and (C) 68−73−79. In panel A, the solid line represents the as-isolated protein (423 μM), while the dashed line represents the reconstituted protein (344 μM). In panels B (1.3 mM protein) and C (395 μM protein), the solid line represents as-isolated triple variants, while the dashed line is a scaled overlay of the WT protein for comparison. Each sample was incubated at room temperature in the presence of 2 mM sodium dithionite for ~2 min before freezing in liquid nitrogen. Conditions of measurement were as follows: microwave power, 5 mW; receiver gain, 2×10^4; modulation amplitude, 10 G; temperature, 13 K; microwave frequency, 9.48 GHz.

catalyzing formation of LHP or 5′-dA. By contrast, the AI WT enzyme catalyzed formation of 13.6 μM LHP and 30 μM 5′-dA (0.27 and 0.60 equiv per polypeptide, respectively) after 20 min at 37 °C, while the reconstituted enzyme catalyzed formation of 17.7 μM LHP and 48 μM 5′-dA (0.36 and 0.96 equiv per polypeptide, respectively). For both AI and RCN enzymes, the formation of both products could be fitted to a first-order kinetic equation, yielding similar rate constants (~0.18 min^{-1}). In addition, the ratio of 5′-dA to LHP, which has been addressed in a previous

Table 2: Equivalents of Iron and Sulfide and Activity of Various LS Samples[a]

sample	ratio (A_{280}/A_{412})	equiv of iron per polypeptide	equiv of sulfide per polypeptide	5′-dA (μM)[b]	LHP (μM)[b]
wild-type AI	2.88	6.9 ± 0.5	6.4 ± 0.9	30.0	13.6
wild-type RCN	2.04	13.8 ± 0.6	13.1 ± 0.2	48.0	17.7
C68A−C73A−C79A AI	4.36	3.0 ± 0.2	3.6 ± 0.4	*c*	*c*
C68A−C73A−C79A RCN	3.00	4.8 ± 0.1	3.6 ± 0.2	*c*	*c*
C94A−C98A−C101A AI	5.00	4.2 ± 0.1	4.7 ± 0.8	*c*	*c*
C94A−C98A−C101A RCN	2.50	10.1 ± 0.4	10.0 ± 0.8	*c*	*c*

[a] Values are for WT LS and variants expressed in M9 minimal medium containing 50 μM ^{57}Fe and are the average of four determinations. [b] All assays were performed with 50 μM WT or variant LS, and the values reported are after a 20-min incubation at 37 °C. [c] Not detected (based on the limit of detection).

publication (*21*), did not differ significantly between the two proteins.

DISCUSSION

Until recently, the in vitro characterization of the LS reaction has been impeded by the unknown nature of the true substrates for the reaction (*20, 21*). Accordingly, given the similarities that the two enzymes share, studies on BS have served as a general model for catalysis by LS. In both systems, the 5′-deoxyadenosyl radicals generated from the cleavage of SAM are believed to remove unactivated hydrogen atoms from the respective substrates to allow for subsequent sulfur insertion. At present, the major issues and points of contention with respect to catalysis by BS relate to cofactor composition of the protein, the exact nature of the immediate sulfur donor, and the chemistry by which the sulfur atom in biotin is inserted.

Studies from Marquet's laboratory provided initial evidence that the source of the sulfur atom in biotin derived from the protein itself and was most likely an Fe/S cluster (*74*). Consistent with this finding, results from Jarrett's laboratory suggested that the "active" form of BS contained two distinct cluster configurations on each polypeptide. A [4Fe−4S] cluster, housed in the C−X_3−C−X_2−C motif, was postulated to interact with SAM in the presence of a suitable reductant to generate the 5′-dA$^{\bullet}$, while a [2Fe−2S] cluster was proposed to serve as the source of the sulfur that is incorporated into the substrate (*48, 75*). This proposal was largely based on the UV−visible spectrum of the protein and the changes observed in the spectrum during turnover. A number of spectroscopic studies on BS, including in vivo Mössbauer experiments (*54, 55*), as well as Mössbauer, resonance Raman, and crystallographic studies on purified and reconstituted enzyme (*33, 49, 50, 65, 76*), have confirmed the presence of both Fe/S clusters on active BS. In addition, it has been demonstrated spectroscopically that SAM interacts with the [4Fe−4S] cluster, thus corroborating the proposed role for this cluster in the generation of the 5′-dA$^{\bullet}$ (*32*). The premise that active BS contains two distinct cluster types is not universally shared (*56, 77*); the mechanism of sulfur insertion from the $[2Fe-2S]^{2+}$ cluster is presently only speculative (*48*), and indeed there is no compelling evidence that the *intact* [2Fe−2S] cluster is the immediate sulfur donor (*50, 65*).

In this study, we endeavored to ascertain whether the parallels between BS and LS could be extended to the number of Fe/S clusters per polypeptide as well as their configuration. We employed a combination of spectroscopic methods (Mössbauer, EPR, and UV−visible), analytical methods (iron, sulfide, and protein quantification), and activity assays on WT LS and two triple variants, in which the three cysteine residues residing in either the C−X_3−C−X_2−C motif or the C−X_4−C−X_5−C motif were changed to alanine. Importantly, all of our studies were carried out on proteins that were expressed in the presence of ^{57}Fe—and sometimes further reconstituted with ^{57}Fe and sulfide—to relate the quantity of bound iron to cluster configuration. Our results indicate that LS houses two [4Fe−4S] clusters per polypeptide; one cluster is ligated by the cysteines in the radical SAM C−X_3−C−X_2−C motif, while the other is ligated by the cysteines in the C−X_4−C−X_5−C motif, which is unique to LSs. Perhaps the most significant finding, especially in light of the ongoing studies on BS, is that LS, when isolated anaerobically from cells in which it and the *A. vinelandii isc* operon are coexpressed, is active without in vitro reconstitution. This has also been observed prior to this study, although the amount of turnover was significantly less (*22*).

In the original characterization of LS, it was reported that the AI protein contained 1.8 ± 0.2 equiv of Fe and 2.2 ± 0.4 equiv of S^{2-} per polypeptide (*38*), while a later characterization of the enzyme, which included assessment of enzymatic turnover, indicated that AI monomeric LS contained 3.4 ± 0.4 equiv of Fe and 4.8 ± 0.8 equiv of S^{2-} and that AI dimeric LS contained 3.3 ± 0.4 equiv of Fe and 4.2 ± 0.5 equiv of S^{2-} per polypeptide (*22*). LS that was purified from inclusion bodies and reconstituted with a 6-fold excess of iron and sulfide was purported to contain 1.8−2.3 equiv of Fe and S^{2-} per polypeptide in one instance (*39*) and 3.7−4.2 mol of Fe and S^{2-} in the other (*69*). Last, LS that was isolated from an expression system containing a plasmid that encodes the *E. coli isc* operon was purported to contain 3.4−3.6 equiv of Fe and 2.4 equiv of S^{2-} per polypeptide (*64*). In this study, we find that AI WT LS, purified from a similar expression system but in minimal media containing ^{57}Fe, contains 6.9 ± 0.5 equiv of Fe and 6.4 ± 0.9 equiv of S^{2-} per polypeptide, almost enough for two [4Fe−4S] clusters in each polypeptide.

Because our stoichiometry depends largely on the ability to quantify protein concentration accurately, we went to significant extents to ensure that our correction factor for the Bradford protein assay was appropriate. We found that the Bradford protein determination method using BSA as a standard overestimates the concentration of LS by a factor of 1.47 ± 0.27. In an earlier study it was reported that the same protein assay overestimates the concentration of LS by 92% (*22*). If we were to use that correction factor our Fe

and S^{2-} stoichiometry would increase, not decrease, resulting in 9.0 Fe and 8.3 S^{2-} per polypeptide. Moreover, we have addressed the stoichiometry of the LS reaction with respect to SAM usage and find that each polypeptide catalyzes formation of almost exactly one equiv of 5′-dA in a pseudo-first-order kinetic process when using a Bradford correction factor of 1.47 ± 0.27 (*21*).

Upon reconstitution of AI WT LS, the quantity of iron and sulfide bound to the protein increases significantly to 13.8 ± 0.6 and 13.1 ± 0.2 per polypeptide; however, Mössbauer spectroscopy reveals that only ∼9.2 ± 1.2 irons are in the configuration $[4Fe-4S]^{2+}$, giving rise to 2.3 ± 0.3 clusters per polypeptide with the remainder existing presumably as adventitiously bound species. Importantly, the 1.4-fold increase in the $[4Fe-4S]^{2+}$ stoichiometry of RCN WT LS as compared to AI WT LS correlates well with the increase in activity of the protein; a 1.6-fold increase in 5′-dA and a 1.3-fold increase in LHP is observed after 20 min at 37 °C.

Importantly, both triple variants, whether reconstituted or not, were completely inactive with respect to formation of 5′-dA and LHP, thus demonstrating that both [4Fe−4S] clusters are essential for turnover. Our finding that 68−73−79 does not promote reductive cleavage of SAM may be unexpected, since this variant has the $C-X_3-C-X_2-C$ cluster intact, which is the cluster that is proposed to function intimately in generation of the 5′-dA•. Studies by Mulliez et al. have demonstrated that reduction of the $[4Fe-4S]^{2+}$ cluster of the activating enzyme (AE) of the ARR is highly coupled to a thermodynamically favorable step, which in that system is generation of the glycyl radical on the ARR (*78*). In LS, abstraction of a hydrogen atom from the octanoyl moiety of OHP to afford a primary alkyl radical would not be considered to be suitably downhill; the thermodynamically favorable step would most likely be the subsequent one, which we hypothesize to be the interaction of the alkyl radical with the sulfur donor. We posit that the activated form of the sulfur donor in 68−73−79 is not present.

Recently, it has been shown that the [2Fe−2S] cluster of BS decays during biotin formation (*48*, *65*), suggesting that it is the immediate sulfur donor or that it is converted into the immediate sulfur donor. We speculate that in LS the cluster that is coordinated by the $C-X_4-C-X_5-C$ motif may play a similar role, somehow supplying the sulfur atoms that are incorporated into the substrate. There is a clear difference between BS and LS, since both clusters in LS are [4Fe−4S] clusters, whereas BS contains one [2Fe−2S] cluster and one [4Fe−4S] cluster. Although BS is typically purified aerobically, wherein only the [2Fe−2S] cluster is present, it was recently shown that this cluster form is also present in vivo and after anaerobic isolation of the protein, suggesting that the [2Fe−2S] cluster of aerobically purified BS is not caused by oxidative damage of a [4Fe−4S] cluster (*50*, *54*, *55*). It is tempting to speculate that the difference in cluster type between BS and LS may reflect the different requirements for sulfur in the respective reactions, in that only one sulfur atom is required for formation of biotin from dethiobiotin, whereas formation of the lipoyl group requires addition of two sulfur atoms to an octanoyl chain. Our recent experiments on LS indicate, however, that formation of one lipoyl group is catalyzed by two LS molecules, suggesting that each LS polypeptide provides only one sulfur atom for generation of the lipoyl group.

In conclusion, we have unambiguously demonstrated that (1) active LS binds two distinct [4Fe−4S] clusters per polypeptide and (2) both clusters are vital for converting OHP to LHP. Furthermore, these results set the stage for more detailed studies to elucidate the functional role of each of the clusters, which are presently ongoing in our laboratories.

ACKNOWLEDGMENT

We are indebted to Dr. Dennis R. Dean (Virgina Tech University) for the gift of plasmid pDB1282.

REFERENCES

1. Biewenga, G. P., Haenen, G. R. M. M., and Bast, A. (1997) An overview of lipoate chemistry, in *Lipoic Acid in Health and Disease* (Fuchs, J., Packer, L., and Zimmer, G., Eds.) pp 1−32, Marcel Dekker, Inc., New York.
2. Douce, R., Bourguignon, J., Macherel, D., and Neuburger, M. (1994) The glycine decarboxylase system in higher plant mitochondria: Structure, function and biogenesis, *Biochem. Soc. Trans. 22*, 184−188.
3. Pares, S., Cohen-Addad, C., Sieker, L., Neuburger, M., and Douce, R. (1994) X-ray structure determination at 2.6-Å resolution of a lipoate-containing protein: The H-protein of the glycine decarboxylase complex from pea leaves, *Proc. Natl. Acad. Sci. U.S.A. 914*, 4850−4853.
4. Reed, L. (1974) Multienzyme complexes, *Acc. Chem. Res. 7*, 40−46.
5. Reed, L. J., Busk, B. G. D., Gunsalus, I. C., and Schnakenberg, G. H. F. (1951) Crystalline α-lipoic acid: A catalytic agent associated with pyruvate dehydrogenase, *Science 114*, 93.
6. Reed, L. J., and Hackert, M. L. (1990) Structure−function relationships in dihydrolipoamide acyltransferases, *J. Biol. Chem. 265*, 8971−8974.
7. Williams, C. H. (1992) Lipoamide dehydrogenase, glutathionine reductase, thioredoxin reductase and mercuric reductase-family of flavoenzyme transhydrogenases, in *Chemistry and Biochemistry of Flavoproteins* (Müller, F., Ed.) pp 121−211, CRC Press, Boca Raton, FL.
8. Robinson, J. R., Klein, S. M., and Sagers, R. D. (1973) Glycine metabolism. Lipoic acid as the prosthetic group in the electron-transfer protein P2 from *Peptococcus glycinophilus*, *J. Biol. Chem. 248*, 5319−5323.
9. Fujiwara, K., and Motokawa, Y. (1983) Mechanism of the glycine cleavage reaction. Steady-state kinetic studies of the P-protein-catalyzed reaction, *J. Biol. Chem. 258*, 8156−8162.
10. Klein, S. M., and Sagers, R. D. (1967) Glycine metabolism. III. A flavin-linked dehydrogenase associated with the glycine cleavage system in *peptococcus glycinophilus*, *J. Biol. Chem. 242*, 297−300.
11. Klein, S. M., and Sagers, R. D. (1966) Glycine metabolism. II. Kinetic and optical studies on the glycine decarboxylase system from *Peptococcus glycinophilus*, *J. Biol. Chem. 241*, 206−209.
12. Klein, S. M., and Sagers, R. D. (1966) Glycine metabolism. I. Properties of the system catalyzing the exchange of bicarbonate with the carboxyl group of glycine in *Peptococcus glycinophilus*, *J. Biol. Chem. 241*, 197−205.
13. Fujiwara, K., Okamura-Ikeda, K., and Motokawa, Y. (1984) Mechanism of the glycine cleavage reaction. Further characterization of the intermediate attached to H-protein and of the reaction catalyzed by T-protein, *J. Biol. Chem. 259*, 10664−10668.
14. Morris, T. W., Reed, K. E., and Cronan, J. E., Jr. (1995) Lipoic acid metabolism in *Escherichia coli*: The *lplA* and *lipB* genes define redundant pathways for ligation of lipoyl groups to apoprotein, *J. Bacteriol. 177*, 1−10.
15. Green, D. E., Morris, T. W., J., G., Cronan, J. E., Jr. and Guest, J. R. (1995) Purification and properties of the lipoate protein ligase of *Escherichia coli*, *Biochem. J. 309*, 853−862.
16. Morris, T. W., Reed, K. E., and Cronan, J. E., Jr. (1994) Identification of the gene encoding lipoate-protein ligase of *Escherichia coli*. Molecular cloning and characterization of the *lplA* gene and gene product, *J. Biol. Chem. 269*, 16091−16100.

17. Jordan, S. W., and Cronan, J. E., Jr. (1997) A new metabolic link. The acyl carrier protein of lipid synthesis donates lipoic acid to the pyruvate dehydrogenase complex in *Escherichia coli* and mitochondria, *J. Biol. Chem. 272*, 17903−17906.
18. Jordan, S. W., and Cronan, J. E., Jr. (1997) Biosynthesis of lipoic acid and posttranslational modification with lipoic acid in *Escherichia coli*, *Methods Enzymol. 279*, 176−183.
19. Jordan, S. W., and Cronan, J. E., Jr. (2003) The *Escherichia coli lipB* gene encodes lipoyl (octanoyl)-acyl carrier protein:protein transferase, *J. Bacteriol. 185*, 1582−1589.
20. Zhao, S., Miller, J. R., Jiang, Y., Marletta, M. A., and Cronan, J. E., Jr. (2003) Assembly of the covalent linkage between lipoic acid and its cognate enzymes, *Chem. Biol. 10*, 1293−1302.
21. Cicchillo, R. M., Iwig, D. F., Jones, A. D., Nesbitt, N. M., Baleanu-Gogonea, C., Souder, M. G., Tu, L., and Booker, S. J. (2004) Lipoyl synthase requires two equivalents of *S*-adenosyl-L-methionine to synthesize one equivalent of lipoic acid, *Biochemistry 43*, 6378−6386.
22. Miller, J. R., Busby, R. W., Jordan, S. W., Cheek, J., Henshaw, T. F., Ashley, G. W., Broderick, J. B., Cronan, J. E., Jr. and Marletta, M. A. (2000) *Escherichia coli* LipA is a lipoyl synthase: In vitro biosynthesis of lipoylated pyruvate dehydrogenase complex from octanoyl-acyl carrier protein, *Biochemistry 39*, 15166−15178.
23. Frey, P. A., and Magnusson, O. T. (2003) *S*-Adenosylmethionine: A wolf in sheep's clothing, or a rich man's adenosylcobalamin? *Chem. Rev. 103*, 2129−2148.
24. Frey, P. A., and Booker, S. (1999) Radical intermediates in the reaction of lysine 2,3-aminomutase, in *Advances in Free Radical Chemistry* (Zard, S. Z., Ed.) pp 1−43, JAI Press Inc., Stamford, CT.
25. Cheek, J., and Broderick, J. B. (2001) Adenosylmethionine-dependent iron−sulfur enzymes: Versatile clusters in a radical new role, *J. Biol. Inorg. Chem. 6*, 209−226.
26. Sofia, H. J., Chen, G., Hetzler, B. G., Reyes-Spindola, J. F., and Miller, N. E. (2001) Radical SAM, a novel protein superfamily linking unresolved steps in familiar biosynthetic pathways with radical mechanisms: Functional characterization using new analysis and information visualization methods, *Nucleic Acids Res. 29*, 1097−1106.
27. Henshaw, T. F., Cheek, J., and Broderick, J. B. (2000) The [4Fe-4S]$^{+1}$ cluster of pyruvate formate-lyase activating enzyme generates the glycyl radical on pyruvate formate-lyase: EPR-detected single turnover, *J. Am. Chem. Soc. 122*, 8331−8332.
28. Lieder, K. W., Booker, S., Ruzicka, F. J., Beinert, H., Reed, G. H., and Frey, P. A. (1998) *S*-Adenosylmethionine-dependent reduction of lysine 2,3-aminomutase and observation of the catalytically functional iron−sulfur centers by electron paramagnetic resonance, *Biochemistry 37*, 2578−2585.
29. Ollagnier-de-Choudens, S., Sanakis, Y., Hewitson, K. S., Roach, P., Münck, E., and Fontecave, M. (2002) Reductive cleavage of *S*-adenosylmethionine by biotin synthase from *Escherichia coli*, *J. Biol. Chem. 277*, 13449−13454.
30. Ollagnier, S., Mulliez, E., Schmidt, P. P., Eliasson, R., Gaillard, J., Deronzier, C., Bergman, T., Gräslund, A., Reichard, P., and Fontecave, M. (1997) Activation of the anaerobic ribonucleotide reductase from *Escherichia coli*. The essential role of the iron−sulfur center for S-adenosylmethionine reduction, *J. Biol. Chem. 272*, 24216−24223.
31. Chen, D., Walsby, C., Hoffman, B. M., and Frey, P. A. (2003) Coordination and mechanism of reversible cleavage of S-adenosylmethionine by the [4Fe-4S] center in lysine 2,3-aminomutase, *J. Am. Chem. Soc. 125*, 11788−11789.
32. Cosper, M. M., Jameson, G. N. L., Davydov, R., Eidsness, M. K., Hoffman, B. M., Huynh, B. H., and Johnson, M. K. (2002) The [4Fe-4S]$^{2+}$ cluster in reconstituted biotin synthase binds *S*-adenosyl-L-methionine, *J. Am. Chem. Soc. 124*, 14006−14007.
33. Berkovitch, F., Nicolet, Y., Wan, J. T., Jarrett, J. T., and Drennan, C. L. (2004) Crystal structure of biotin synthase, an S-adenosylmethionine-dependent radical enzyme, *Science 303*, 76−79.
34. Walsby, C. J., Ortillo, D., E., B. W., Broderick, J. B., and Hoffman, B. M. (2002) An anchoring role for FeS clusters: Chelation of the amino acid moiety of *S*-adenosylmethionine to the unique iron site of the [4Fe-4S] cluster of pyruvate formate-lyase activating enzyme, *J. Am. Chem. Soc. 124*, 11270−11271.
35. Walsby, C. J., Hong, W., Broderick, W. E., Cheek, J., Ortillo, D., Broderick, J. B., and Hoffman, B. M. (2002) Electron−nuclear double resonance spectroscopic evidence that *S*-adenosylmethionine binds in contact with the catalytically active [4Fe-4S]$^{+}$ cluster of pyruvate formate-lyase activating enzyme, *J. Am. Chem. Soc. 124*, 3143−3151.
36. Layer, G., Moser, J., Heinz, D. W., Jahn, D., and Schubert, W. D. (2003) Crystal structure of coproporphyrinogen III oxidase reveals cofactor geometry of radical SAM enzymes, *EMBO J. 22*, 6214−6224.
37. Krebs, C., Broderick, W. E., Henshaw, T. F., Broderick, J. B., and Huynh, B. H. (2002) Coordination of adenosylmethionine to a unique iron site of the [4Fe-4S] of pyruvate formate-lyase activating enzyme: A Mössbauer spectroscopic study, *J. Am. Chem. Soc. 124*, 912−913.
38. Busby, R. W., Schelvis, J. P. M., Yu, D. S., Babcock, G. T., and Marletta, M. A. (1999) Lipoic acid biosynthesis: LipA is an iron sulfur protein, *J. Am. Chem. Soc. 121*, 4706−4707.
39. Ollagnier-de Choudens, S., and Fontecave, M. (1999) The lipoate synthase from *Escherichia coli* is an iron−sulfur protein, *FEBS Lett. 453*, 25−28.
40. Parry, R. J. (1983) Biosynthesis of some sulfur-containing natural products. Investigations of the mechanism of carbon−sulfur bond formation, *Tetrahedron 39*, 1215−1238.
41. Marquet, A. (2001) Enzymology of carbon−sulfur bond formation, *Curr. Opin. Chem. Biol. 5*, 541−549.
42. Fontecave, M., Mulliez, E., and Ollagnier-de Choudens, S. (2001) Adenosylmethionine as a source of 5′-deoxyadenosyl radicals, *Curr. Opin. Chem. Biol. 5*, 506−511.
43. Jarrett, J. T. (2003) The generation of 5′-deoxyadenosyl radicals by adenosylmethionine-dependent radical enzymes, *Curr. Opin. Chem. Biol. 7*, 174−182.
44. Hayden, M. A., Huang, I., Bussiere, D. E., and Ashley, G. W. (1992) The biosynthesis of lipoic acid: Cloning of *lip*, a lipoate biosynthetic locus of *Escherichia coli*, *J. Biol. Chem. 267*, 9512−9515.
45. Reed, K. E., and Cronan, J. E., Jr. (1993) Lipoic acid metabolism in *Escherichia coli*: Sequencing and functional characterization of the *lipA* and *lipB* genes, *J. Bacteriol. 175*, 1325−1336.
46. Otsuka, A. J., Buoncristiani, M. R., Howard, P. K., Flamm, J., Johnson, C., Yamamoto, R., Uchida, K., Cook, C., Ruppert, J., and Matsuzaki, J. (1988) The *Escherichia coli* biotin biosynthetic enzyme sequences predicted from the nucleotide sequence of the *bio* operon, *J. Biol. Chem. 263*, 19577−19585.
47. Hewitson, K. S., Ollagnier-de Choudens, S., Sanakis, Y., Shaw, N. M., Baldwin, J. E., Münck, E., Roach, P. L., and Fontecave, M. (2002) The iron-suflur center of biotin synthase: Site-directed mutants, *J. Biol. Inorg. Chem. 7*, 83−93.
48. Ugulava, N. B., Sacanell, C. J., and Jarrett, J. T. (2001) Spectroscopic changes during a single turnover of biotin synthase: Destruction of a [2Fe-2S] cluster accompanies sulfur insertion, *Biochemistry 40*, 8352−8358.
49. Ugulava, N. B., Surerus, K. K., and Jarrett, J. T. (2002) Evidence from Mössbauer spectroscopy for distinct [2Fe-2S]$^{2+}$ and [4Fe-4S]$^{2+}$ cluster binding sites in biotin synthase from *Escherichia coli*, *J. Am. Chem. Soc. 124*, 9050−9051.
50. Cosper, M. M., Jameson, G. N. L., Hernández, H. L., Krebs, C., Huynh, B. H., and Johnson, M. K. (2004) Characterization of the cofactor composition of *Escherichia coli* biotin synthase, *Biochemistry 43*, 2007−2021.
51. Duin, E. C., Lafferty, M. E., Crouse, B. R., Allen, R. M., Sanyal, I., Flint, D. H., and Johnson, M. K. (1997) [2Fe-2S] to [4Fe-4S] cluster conversion in *Escherichia coli* biotin synthase, *Biochemistry 36*, 11811−11820.
52. Sanyal, I., Cohen, G., and Flint, D. H. (1994) Biotin synthase: Purification, characterization as a [2Fe-2S] cluster protein, and in vitro activity of the *Escherichia coli bioB* gene product, *Biochemistry 33*, 3625−3631.
53. Tse Sum Bui, B., Florentin, D., Marquet, A., Benda, R., and Trautwein, A. X. (1999) Mössbauer studies of *Escherichia coli* biotin synthase: Evidence for reversible interconversion between [2Fe-2S]$^{2+}$ and [4Fe-4S]$^{2+}$ clusters, *FEBS Lett. 459*, 411−414.
54. Cosper, M. M., Jameson, G. N. L., Eidsness, M. K., Huynh, B. H., and Johnson, M. K. (2002) Recombinant *Escherichia coli* biotin synthase is a [2Fe-2S]$^{2+}$ protein in whole cells, *FEBS Lett. 529*, 332−336.
55. Benda, R., Tse Sum Bui, B., Schünemann, V., Florentin, D., Marquet, A., and Trautwein, A. X. (2002) Iron−sulfur clusters of biotin synthase in vivo: A Mössbauer study, *Biochemistry 41*, 15000−15006.
56. Ollagnier-de Choudens, S., Mulliez, E., Hewitson, K. S., and Fontecave, M. (2002) Biotin synthase is a pyridoxal phosphate-dependent cysteine desulfurase, *Biochemistry 41*, 9145−9152.

57. Beinert, H. (1978) Micro methods for the quantitative determination of iron and copper in biological material, *Methods Enzymol. 54*, 435−445.
58. Beinert, H. (1983) Semi-micro methods for analysis of labile sulfide and of labile sulfide plus sulfane sulfur in unusually stable iron−sulfur proteins, *Anal. Biochem. 131*, 373−378.
59. Kennedy, M. C., Kent, T. A., Emptage, M., Merkle, H., Beinert, H., and Münck, E. (1984) Evidence for the formation of a linear [3Fe-4S] cluster in partially unfolded aconitase, *J. Biol. Chem. 259*, 14463−14471.
60. Sambrook, J., Fritsch, E. F., and Maniatis, T. (1989) *Molecular cloning: A Laboratory Manual*, 2nd ed., Vol. 3, Cold Spring Harbor Laboratory Press, Plainview, NY.
61. Ramamurthy, V., Swann, S. L., Paulson, J. L., Spedaliere, C. J., and Mueller, E. G. (1999) Critical aspartic acid residues in pseudouridine synthases, *J. Biol. Chem. 274*, 22225−22230.
62. Frazzon, J., and Dean, D. R. (2003) Formation of iron−sulfur clusters in bacteria: An emerging field in bioinorganic chemistry, *Curr. Opin. Chem. Biol. 7*, 166−173.
63. Frazzon, J., Fick, J. R., and Dean, D. R. (2002) Biosynthesis of iron-sulphur clusters is a complex and highly conserved process, *Biochem. Soc. Trans. 30*, 680−685.
64. Kriek, M., Peters, L., Takahashi, Y., and Roach, P. L. (2003) Effect of iron−sulfur cluster assembly proteins on the expresssion of *Escherichia coli* lipoic acid synthase, *Protein Expression Purif. 28*, 241−245.
65. Jameson, G. N. L., Cosper, M. M., Hernández, H. L., Johnson, M. K., and Huynh, B. H. (2004) Role of the [2Fe-2S] cluster in recombinant *Escherichia coli* biotin synthase, *Biochemistry 43*, 2022−2031.
66. Nakamura, A., and Ueyama, N. (1994) Iron−sulfur models of protein active sites, in *Encyclopedia of Inorganic Chemistry* (King, R. B., Ed.) pp 1883−1896, John Wiley & Sons, Chichester, U.K.
67. Holm, R. H., and Ibers, J. A. (1977) Synthetic analogues of the active sites of iron−sulfur proteins, in *Iron−Sulfur Proteins* (Lovenberg, W., Ed.), Academic Press, New York.
68. Orme-Johnson, W. H., and Orme-Johnson, N. R. (1982) Iron−sulfur proteins: The problem of determining cluster type, in *Iron−Sulfur Proteins* (Spiro, T. G., Ed.) John Wiley & Sons, New York.
69. Ollagnier-de Choudens, S., Sanakis, Y., Hewitson, K. S., Roach, P., Baldwin, J. E., Münck, E., and Fontecave, M. (2000) Iron−sulfur center of biotin synthase and lipoate synthase, *Biochemistry 39*, 4165−4173.
70. Kent, T. A., Huynh, B. H., and Münck, E. (1980) Iron−sulfur proteins: Spin-coupling model for three-iron clusters, *Proc. Natl. Acad. Sci. U.S.A. 77*, 6574−6576.
71. Papaefthymiou, V., Girerd, J. J., Moura, J. J. G., Moura, E., and Münck, E. (1987) Mössbauer study of *D. gigas* ferredoxin II and spin-coupling model for Fe_3S_4 cluster with valence delocalization, *J. Am. Chem. Soc. 109*, 4703−4710.
72. Krebs, C., Henshaw, T. F., Cheek, J., Huynh, B. H., and Broderick, J. B. (2000) Conversion of 3Fe-4S to 4Fe-4S clusters in native pyruvate formate-lyase activating enzyme: Mössbauer characterization and implications for mechanism, *J. Am. Chem. Soc. 122*, 12497−12506.
73. Külzer, R., Pils, T., Kappl, R., Hüttermann, J., and Knappe, J. (1998) Reconstitution and characterization of the polynuclear iron−sulfur cluster in pyruvate formate-lyase-activating enzyme, *J. Biol. Chem. 273*, 4897−4903.
74. Tse Sum Bui, B., Florentin, B., Fournier, F., Ploux, O., Méjean, A., and Marquet, A. (1998) Biotin synthase mechanism: On the origin of sulphur, *FEBS Lett. 440*, 226−230.
75. Ugulava, N. B., Gibney, B. R., and Jarrett, J. T. (2001) Biotin synthase contains two distinct iron−sulfur binding sites: Chemical and spectroelectrochemical analysis of iron−sulfur cluster interconversions, *Biochemistry 40*, 8343−8351.
76. Tse Sum Bui, B., Benda, R., Schünemann, V., Florentin, D., Trautwein, A. X., and Marquet, A. (2003) Fate of the $(2Fe\text{-}2S)^{2+}$ cluster of *Escherichia coli* biotin synthase during reaction: A Mössbauer characterization, *Biochemistry 42*, 8791−8798.
77. Ollagnier-de Choudens, S., Mulliez, E., and Fontecave, M. (2002) The PLP-dependent biotin synthase from *Escherichia coli*: Mechanistic studies, *FEBS Lett. 532*, 465−468.
78. Mulliez, E., Padovani, D., Atta, M., Alcouffe, C., and Fontecave, M. (2001) Activation of class II ribonucleotide reductase by flavodoxin: A protein radical-driven electron transfer to the iron−sulfur center, *Biochemistry 40*, 3730−3736.

BI0488505